Available online at www.sciencedirect.com
SCIENCE DIRECT®
Journal of Solid State Chemistry 177 (2004) 2705–2713
JOURNAL OF SOLID STATE CHEMISTRY
http://elsevier.com/locate/jssc

A new layered organically templated iron(II) phosphite, $(C_2H_{10}N_2)[Fe_3(HPO_3)_4]$. Hydrothermal synthesis, crystal structure and spectroscopic and magnetic properties

U-Chan Chung,[a] José L. Mesa,[b,*] José L. Pizarro,[a] Luis Lezama,[b] José S. Garitaonandia,[c] Jon P. Chapman,[b] and María I. Arriortua[a]

[a] *Facultad de Ciencia y Tecnologia, Departamento de Mineralogía-Petrología, Universidad del País Vasco, Apdo. 644, E-48080 Bilbao, Spain*
[b] *Facultad de Ciencia y Tecnologia, Departamento de Química Inorgánica, Universidad del País Vasco, Apdo. 644, E-48080 Bilbao, Spain*
[c] *Facultad de Ciencia y Tecnologia, Departamento de Física Aplicada II, Universidad del País Vasco, Apdo. 644, E-48080 Bilbao, Spain*

Received 19 November 2003; received in revised form 30 January 2004; accepted 4 April 2004

Abstract

The $(C_2H_{10}N_2)[Fe_3(HPO_3)_4]$ compound has been synthesized by using mild hydrothermal conditions under autogeneous pressure and the ethylenediamine molecule as templating agent. The compound crystallizes in the triclinic $P\bar{1}$ space group with unit-cell parameters $a = 5.416(1)$, $b = 5.416(1)$, $c = 13.977(2)$ Å, $\alpha = 80.64(2)$, $\beta = 85.25(1)$, $\gamma = 60.03(1)^\circ$ and $Z = 1$. The final R-factors were $R_1 = 0.053$ [w$R_2 = 0.092$]. The crystal structure is constructed of layers stacked along the c-axis. The sheets contain FeO_6 octahedra linked by $(HPO_3)^{2-}$ phosphite oxoanions to give rise to Fe_3O_{12} trimeric units sharing faces. The IR spectrum shows the characteristic bands of the phosphite and ethylenediammonium ions. From the diffuse reflectance spectrum, the Dq parameter of 805 cm^{-1} has been calculated for the iron(II) cation in slightly distorted octahedral geometry. The Mössbauer spectrum exhibits two doublets characteristic of two crystallographically independent iron(II) ions in octahedral symmetry. Magnetic measurements indicate the existence of antiferromagnetic interactions.

Keywords: Hydrothermal synthesis; X-ray diffraction; IR; UV/vis; Mössbauer; Magnetic behavior

1. Introduction

The use of organic compounds as templates when combined with different oxoanions, such as, phosphates, arsenates, phosphites for the generation of inorganic structures and materials, has received increasing attention over the last decade [1]. The transfer of a variety of organic templates to the inorganic products allows the formation of otherwise unattainable inorganic structures [2]. A frequently used concept in seeking systematic trends in this area of materials chemistry is that of templating, the tendency of a cation to direct the reaction to form a particular product [3]. In this way, small organic molecules, particularly those containing protonated amino groups, have played an outstanding role in templating novel networks [4] such as oxides, phosphates, phosphonates with a large variety of transitions metal ions [2].

For over half a century, zeolites have played a major role in the development of modern processes in the chemical and petroleum industries [5]. Their unique combination of physical and chemical properties is ideal for catalysis and separations for a broad range of molecules. The types of microporous materials, tetrahedral- and mixed-framework compounds, with open structures continue to expand in terms of framework-forming elements [2]. The most studied and also largest classes of tetrahedral-framework compounds are alumino-silicates [6], aluminophosphates [7], as well as their isomorphic substituted forms. Attempts to synthesize frameworks with elements other than Al, Si and P, especially with transition metals, have resulted in many new classes, such as gallophosphates, titanosilicates and

*Corresponding author. Fax: 34-946013500.
E-mail address: qipmeruj@lg.ehu.es (J.L. Mesa).

0022-4596/$ - see front matter © 2004 Elsevier Inc. All rights reserved.
doi:10.1016/j.jssc.2004.04.020

beryllium, zinc, cobalt, iron, vanadium, nickel and molybdenum phosphates [8]. Furthermore, compared with tetrahedral elements in zeolitic aluminum silicates (or phosphates), divalent transition metals have a greater coordination flexibility and a stronger tendency to form edge-sharing linkages of metal-oxygen polyhedra.

Among these materials the organically templated iron(III)-phosphates occupy a major position. A number of works dealing with this system has evidenced a considerable structural and compositional diversity [9], being scarce the iron(II) phases. The structural chemistry of phosphite with elements of the first transition series reveals complex two-dimensional and three-dimensional phases [10]. The inorganic–organic hybrid phosphites with metallic transition elements, however, have not been extensively studied, and only compounds with the V(IV), Co(II), Mn(II), Fe(II, III), V(III), Cr(III) cations are known [11]. It is worth mentioning that in the $(C_2H_{10}N_2)[M_3(HPO_3)_4]$ (M^{II} = Mn and Co) family of compounds in which, the metallic cations have similar ionic radius, the protonated ethylenediamine molecule acts as structure directing agent to obtain the same type of layered structural framework [11b,d]. In order to improve the understanding about this type of microporous materials incorporating metallic magnetic cations belonging to the first series of transition elements, we have synthesized the phosphite of formula $(C_2H_{10}N_2)[Fe_3(HPO_3)_4]$. In the present work, we report the synthesis, crystal structure and the thermal and spectroscopic and magnetic properties.

2. Experimental section

2.1. Synthesis and characterization

The $(C_2H_{10}N_2)[Fe_3(HPO_3)_4]$ phase was synthesized under mild hydrothermal conditions starting from reaction mixtures of $FeCl_3 \cdot 6H_2O$ (5.55 mmol), H_3PO_2 hypophosphorous acid (144.8 mmol) and ethylenediamine (0.269 mmol) in a volume of 10 mL of water. The mixture was stirred to assure homogeneity, sealed in a PTFE-lined stainless steel pressure vessel (fill factor 75%) and heated at 170°C for 5 days, followed by slow cooling to room temperature. The pH of the reaction mixture did not show any appreciable change during the hydrothermal reaction and remained at ca. 6.0. This value of pH allows the protonation of the ethylenediamine molecule, incorporated in the form of ethylenediammonium cations, between the $[Fe_3(HPO_3)_4]^{2-}$ inorganic sheets establishing both hydrogen bonds and ionic interactions with these layers. Well formed light-green single-crystals appeared at the end of the synthesis. They were isolated by filtration, washed with water and acetone and dried over P_2O_5 for 2 h. The yield of the reaction was 85%. The percentage of the elements in the product was calculated by inductively coupled plasma atomic emission spectroscopy (ICP-AES) together with C, H, N-elemental analysis. Found: Fe, 30.1; P, 22.1; C, 4.2; H, 2.4; N, 5.0. $(C_2H_{10}N_2)[Fe_3(HPO_3)_4]$ requires Fe, 30.5; P, 22.6; C, 4.4; H, 2.5; N, 5.1. The density of 2.6(1) g cm^{-3} was measured by flotation in a mixture of $CHCl_3/CHBr_3$. A simulation using the pattern matching routine of the FULLPROF program [12],[1] based on the single crystal structure, was in excellent agreement with the X-ray powder data, indicating the presence of a pure phase with high crystallinity.

Thermogravimetric analysis of $(C_2H_{10}N_2)[Fe_3(HPO_3)_4]$ was carried out under oxygen atmosphere in an SDC 2960 Simultaneous DSC-TGA TA Instrument. Crucibles containing ca. 20 mg of sample were heated at 5°C min^{-1} in the temperature range 30–800°C. The decomposition curve reveals a weight loss of 6.2% with superimposed steps between ca. 200°C and 680°C, which correspond to the calcination of the ethylenediammonium dication and the oxidation of the phosphite oxoanion to the phosphate groups, respectively. The X-ray diffraction pattern of the residue obtained after the thermogravimetric analysis at 800°C shows the presence of trigonal Fe(PO_4) [$P3_121$, $a = 5.03(1)$, $c = 11.23(1)$ Å] [13a].

The thermal behavior of $(C_2H_{10}N_2)[Fe_3(HPO_3)_4]$ was also studied using time-resolved X-ray thermodiffractometry in air atmosphere. A PHILIPS X'PERT automatic diffractometer (Cu$K\alpha$ radiation) equipped with a variable-temperature stage (Paar Physica TCU2000) with a Pt sample holder was used in the experiment. The powder patterns were recorded in 2θ steps of 0.02° in the range $4 \leqslant 2\theta \leqslant 40°$, counting for 1 s per step and increasing the temperature at 5°C min^{-1} from room temperature up to 815°C (Fig. 1). The compound is stable up to ca. 195°C and the intensity of the monitored (001) peak at $2\theta = 6.4°$ remains practically unchanged. At around 315°C a strong decrease of the intensity of this peak takes place (ca. 85% of the initial intensity) starting the decomposition of the compound. Between 315°C and 500°C no peaks were observed in the patterns. At temperatures higher than ca. 510°C peaks belonging to the trigonal [$P3_121$, $a = 5.03(1)$, $c = 11.23(1)$ Å] [13a] and orthorhombic [$Cmcm$, $a = 5.23(1)$, $b = 7.70(1)$, $c = 6.32(1)$ Å] [13b] Fe(PO_4) polymorphs are observed. The peaks of the orthorhombic Fe(PO_4) disappear at 585°C and those of $Fe_4(P_2O_7)_3$ appear at 720°C [13c]. These results indicate that the loss of the ethylenediammonium cation gives rise to the collapse of the layered architecture and subsequent formation of various iron(III) phosphates.

[1] The program is a strongly modified version of that described by D.B. Wiles and R.A. Young.

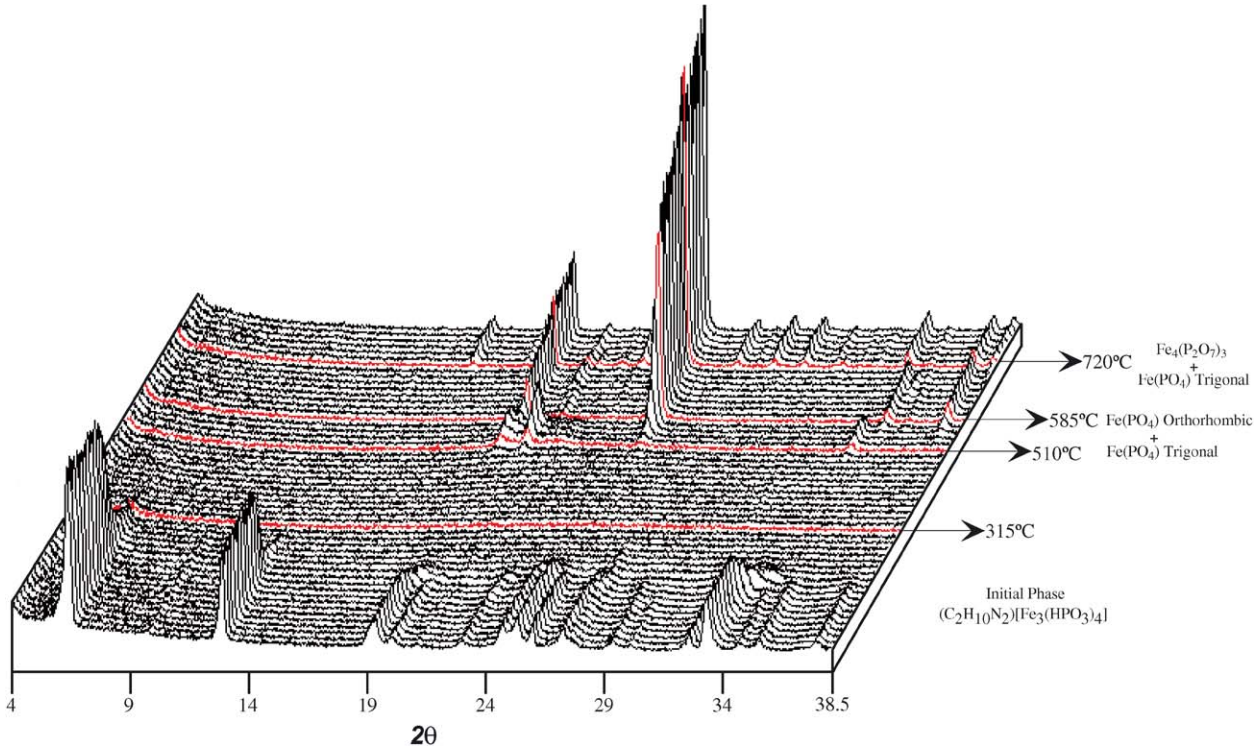

Fig. 1. Thermodiffractograms of $(C_2H_{10}N_2)[Fe_3(HPO_3)_4]$.

2.2. Single-crystal X-ray diffraction

A prismatic single-crystal of $(C_2H_{10}N_2)[Fe_3(HPO_3)_4]$ with dimensions $0.1 \times 0.05 \times 0.05\,mm^3$ was carefully selected under a polarizing microscope and mounted on a glass fiber. Diffraction data were collected at room temperature on an Enraf-Nonius CAD4 automated diffractometer using graphite-monochromated Mo$K\alpha$ radiation. Details of the crystal data, intensity collection and some features of the structure refinement are reported in Table 1. Lattice constants were obtained by a least-squares refinement of the setting angles of 25 reflections in the range $1° < \theta < 30°$. Intensities and angular positions of two standard reflections were measured every hour and showed neither decrease nor misalignment during data collection.

A total of 1579 reflections were measured in the range $1.48 \leqslant 2\theta \leqslant 26.36$ of which 1426 were independent ($R_{int.} = 0.027$) and 1179 observed applying the criterion $I > 2\sigma(I)$. Corrections for Lorentz and polarization effects were made and also for absorption with the empirical ψ scan method [14] using the X-RAYACS program [15]. Direct methods (SHELXS 97) [16] were employed to solve the structure. The metal ions and the phosphorous atoms were first located. The oxygen, nitrogen, and carbon atoms were found in difference Fourier maps. In the crystal structure exist two crystallographically independent iron(II) cations. The Fe(1) ion occupies a special position with an occupancy factor of 0.5. The structure was refined by the full-matrix least-squares method based on F^2, using the SHELXL 97 computer program [17]. The scattering factors were taken from Ref. [18]. All non-hydrogen atoms were assigned anisotropic thermal parameters. The coordinates of hydrogen atoms of the phosphite anion were obtained from difference Fourier maps and those of the

Table 1
Crystallographic data for $(C_2H_{10}N_2)[Fe_3(HPO_3)_4]$

Chemical formula	$C_2H_{14}N_2O_{12}P_4Fe_3$
Molecular weight ($g\,mol^{-1}$)	549.60
Crystal system	Triclinic
Space group	$P\bar{1}$ (no. 2)
a (Å)	5.416(1)
b (Å)	5.416(1)
c (Å)	13.977(2)
α (°)	80.64(2)
β (°)	85.25(1)
γ (°)	60.03(1)
Volume (Å^3)	350.4(1)
Z	1
$\rho_{calcd.}$ ($g\,cm^{-3}$)	2.604
$F(000)$	274
T (K)	293
Radiation, λ(Mo$K\alpha$) (Å)	0.71073
μ (Mo$K\alpha$) (mm^{-1})	3.587
Limiting indices	$-6 \leqslant h \leqslant 5$, $-6 \leqslant k \leqslant 0$, $-17 \leqslant l \leqslant 17$
$R[I > 2\sigma(I)]$	$R_1 = 0.035$; w$R_2 = 0.085$
R [all data]	$R_1 = 0.053$; w$R_2 = 0.092$
Goodness of fit	1.047

$R_1 = [\sum(|F_o| - |F_c|)]/\sum|F_o|$; w$R_2 = [\sum[w(|F_o|^2 - |F_c|^2)^2]/\sum[w(|F_o|^2)^2]]^{1/2}$; $w = 1/[\sigma^2|F_o|^2 + (xp)^2]$; where $p = [|F_o|^2 + 2|F_c|^2]/3$; and $x = 0.065$.

Table 2
Fractional atomic coordinates and equivalent isotropic thermal parameters ($Å^2 \times 10^3$) for $(C_2H_{10}N_2)[Fe_3(HPO_3)_4]$ (e.s.d. in parentheses)

Atom	x/a	y/b	z/c	U_{eq}
Fe(1)	0.0	0.5000	0.0	11(1)
Fe(2)	0.0008(1)	0.4107(1)	0.2110(1)	10(1)
P(1)	0.6671(1)	1.1979(2)	−0.0743(1)	10(1)
P(2)	0.6649(2)	0.0567(2)	0.2633(1)	9(1)
O(1)	0.8189(6)	0.8944(6)	−0.1019(2)	16(1)
O(2)	0.6471(6)	0.6267(6)	0.1019(2)	16(1)
O(3)	0.8304(6)	0.3608(6)	−0.1022(2)	16(1)
O(4)	0.3582(6)	0.2231(6)	0.2983(2)	14(1)
O(5)	0.7913(6)	0.7340(6)	0.2968(2)	16(1)
O(6)	0.8490(6)	0.1659(6)	0.2968(2)	13(1)
N(1)	0.3330(7)	0.6772(7)	0.3779(2)	14(1)
C(1)	0.3651(9)	0.6347(9)	0.4842(3)	21(1)

$$U_{eq} = (1/3)[U_{11}(aa*)^2 + U_{22}(bb*)^2 + U_{33}(cc*)^2 + 2U_{12}aba*b*\cos\gamma + 2U_{13}aca*c*\cos\beta + 2U_{23}bcb*c*\cos\alpha].$$

ethylenediammonium cation were geometrically placed. The final R factors for all data were $R_1 = 0.053$ [w$R_2 = 0.092$]. Maximum and minimum peaks in final difference synthesis were 1.179, $-0.611\,eÅ^{-3}$. The structure factor parameters have been deposited at the Cambridge Crystallographic Data Centre (CCDC 222444). All drawings were made using the ATOMS program [19]. Fractional atomic coordinates and equivalent isotropic thermal parameters are shown in Table 2. Selected bond distances and angles are given in Table 3.

2.3. Physicochemical characterization techniques

The IR spectrum (KBr pellet) was obtained with a Nicolet FT-IR 740 spectrophotometer in the 400–4000 cm^{-1} range. Diffuse reflectance spectrum was registered at room temperature on a Cary 2415 spectrometer in the 210–2000 nm range. Mössbauer measurements were recorded at room temperature in the transmission geometry using a conventional constant-acceleration spectrometer with a ^{57}CoRh source. Magnetic measurements on a powdered sample were performed in the temperature range 5.0–300 K, using a Quantum Design MPMS-7 SQUID magnetometer. The magnetic field was approximately 0.1 T, a value in the range of linear dependence of magnetization vs. magnetic field even at 5.0 K.

Table 3
Selected bond distances (Å) and angles (°) for $(C_2H_{10}N_2)[Fe_3(HPO_3)_4]$ (e.s.d. in parentheses)

Bond distances (Å)			
Fe(1)O$_6$ octahedron		*Fe(2)O$_6$ octahedron*	
Fe(1)–O(1)^{i}/O(1)^{ii}	2.168(3)	Fe(2)–O(1)^{i}	2.229(3)
Fe(1)–O(2)^{i}/O(2)^{ii}	2.170(3)	Fe(2)–O(2)^{ii}	2.242(3)
Fe(1)–O(3)^{i}/O(3)^{ii}	2.171(3)	Fe(2)–O(3)^{i}	2.229(2)
		Fe(2)–O(4)	2.072(3)
		Fe(2)–O(5)^{ii}	2.066(3)
		Fe(2)–O(6)^{ii}	2.069(3)
Fe(1)–Fe(2)/Fe(2)^{iii}	2.9096(7)		
HP(1)O$_3$ tetrahedron		*HP(2)O$_3$ tetrahedron*	
P(1)–O(1)	1.527(3)	P(2)–O(4)	1.524(3)
P(1)–O(2)^{iv}	1.524(3)	P(2)–O(5)^{vi}	1.528(3)
P(1)–O(3)^{v}	1.524(3)	P(2)–O(6)	1.523(3)
H(11)–P(1)	1.31(2)	H(22)–P(2)	1.30(2)
(H$_3$N(CH$_2$)$_2$NH$_3$)$^{2+}$			
N(1)–C(1)	1.477(5)	C(1)–C(1)^{vii}	1.492(8)
Bond angles (°)			
Fe(1)O$_6$ octahedron		*Fe(2)O$_6$ octahedron*	
O(1)^{i}–Fe(1)–O(2)^{i}	97.6(1)	O(5)^{ii}–Fe(2)–O(6)^{ii}	90.4(1)
O(1)^{ii}–Fe(1)–O(2)^{i}	82.4(1)	O(5)^{ii}–Fe(2)–O(4)	90.2(1)
O(1)^{i}–Fe(1)–O(2)^{ii}	82.4(1)	O(6)^{ii}–Fe(2)–O(4)	90.0(1)
O(1)^{ii}–Fe(1)–O(2)^{ii}	97.6(1)	O(5)^{ii}–Fe(2)–O(3)^{i}	96.9(1)
O(1)^{i}–Fe(1)–O(3)^{i}	82.5(1)	O(4)–Fe(2)–O(3)^{i}	93.3(1)
O(1)^{ii}–Fe(1)–O(3)^{i}	97.5(1)	O(6)^{ii}–Fe(2)–O(1)^{i}	92.5(1)
O(2)^{i}–Fe(1)–O(3)^{i}	97.4(1)	O(4)–Fe(2)–O(1)^{i}	97.6(1)
O(2)^{ii}–Fe(1)–O(3)^{i}	82.6(1)	O(3)^{i}–Fe(2)–O(1)^{i}	79.8(1)
O(1)^{i}–Fe(1)–O(3)^{ii}	97.5(1)	O(5)^{ii}–Fe(2)–O(2)^{ii}	92.5(1)
O(1)^{ii}–Fe(1)–O(3)^{ii}	82.6(1)	O(6)^{ii}–Fe(2)–O(2)^{ii}	96.8(1)
O(2)^{i}–Fe(1)–O(3)^{ii}	82.6(1)	O(3)^{i}–Fe(2)–O(2)^{ii}	79.7(1)
O(2)^{ii}–Fe(1)–O(3)^{ii}	97.4(1)	O(1)^{i}–Fe(2)–O(2)^{ii}	79.5(1)
O(1)^{i}–Fe(1)–O(1)^{ii}	180.0(1)	O(6)^{ii}–Fe(2)–O(3)^{i}	172.0(1)
O(2)^{i}–Fe(1)–O(2)^{ii}	180.0(1)	O(5)^{ii}–Fe(2)–O(1)^{i}	171.7(3)
O(3)^{i}–Fe(1)–O(3)^{ii}	180.0(1)	O(4)–Fe(2)–O(2)^{ii}	172.7(1)
HP(1)O$_3$ tetrahedron		*HP(2)O$_3$ tetrahedron*	
O(2)^{iv}–P(1)–O(3)^{v}	113.8(2)	O(6)–P(2)–O(4)	111.3(2)
O(2)^{iv}–P(1)–O(1)	114.2(2)	O(6)–P–O(5)^{vi}	110.7(2)
O(3)^{v}–P(1)–O(1)	113.9(2)	O(4)–P–O(5)^{vi}	110.9(2)
O(2)^{iv}–P(1)–H(11)	102(2)	O(6)–P–H(22)	107(2)
O(3)^{v}–P(1)–H(11)	108(2)	O(4)–P–H(22)	110(2)
O(1)–P(1)–H(11)	104(2)	O(5)^{vi}–P–H(22)	107(2)
(H$_3$N(CH$_2$)2NH$_3$)2+			
N(1)–C(1)–C(1)^{vii}	110.4(4)		

Symmetry codes: i $= -x+1, -y+1, -z$; ii $= x-1, y, z$; iii $= -x, -y+1, -z$; iv $= -x+1, -y+2, -z$; v $= x, y+1, z$; vi $= x, y-1, z$; vii $= -x+1, -y+1, -z+1$.

3. Results and discussion

3.1. Crystal structure of $(C_2H_{10}N_2)[Fe_3(HPO_3)_4$

The $(C_2H_{10}N_2)[Fe_3(HPO_3)_4]$ compound exhibits a layered structure formed by anionic sheets of formula $[Fe_3(HPO_3)_4]^{2-}$, which are extended in the *ab*-plane. The ethylenediammonium cations are located between the layers, compensating their negative charge and establishing hydrogen bonds with the anionic sheets (Fig. 2). The sheets are constructed from iron(II) cations in an octahedral environment, giving rise to trimeric entities with composition Fe_3O_{12} in which the octahedra

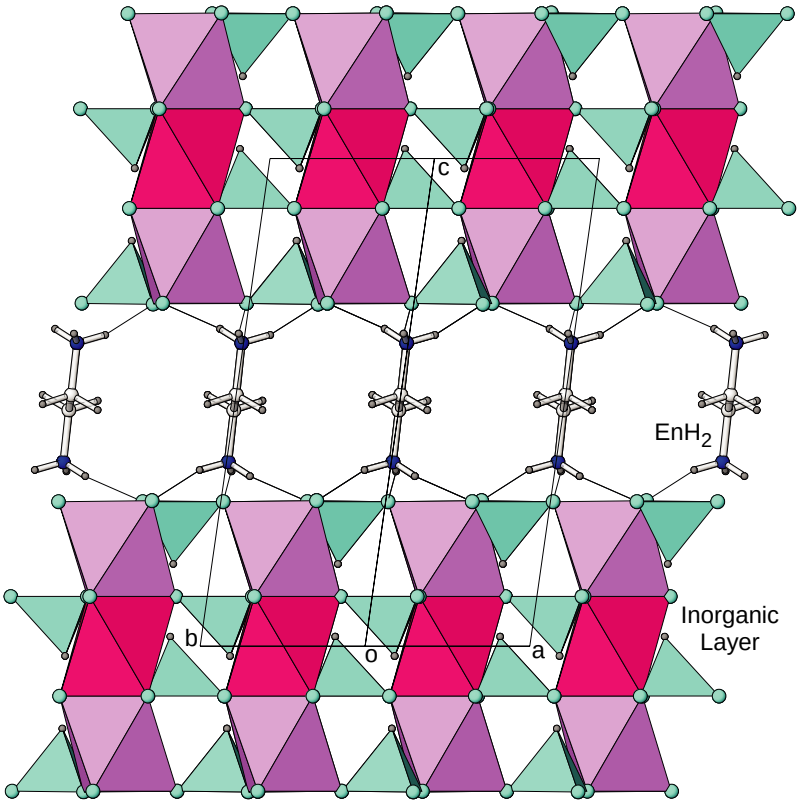

Fig. 2. Polyhedral view along the [110] direction of $(C_2H_{10}N_2)[Fe_3(HPO_3)_4]$, showing the layered structure.

are sharing faces (Fig. 3). The phosphorus(III) ions from the $(HPO_3)^{2-}$ phosphite anions are four-coordinate, with a vertex of the tetrahedron occupied by the hydrogen atom and the others by the oxygen atoms coordinated to the Fe(II) ions. The HPO_3 tetrahedra link the trimeric units, which are extended in the *ab*-plane. The existence of this layered architecture has been also found in the $(C_nH_{2n+6}N_2)$ $[Mn_3(HPO_3)_4]$ $(n = 2-8)$ series of phosphite-compounds and in the $(C_2H_{10}N_2)[Co_3(HPO_3)_4]$ phase [11c,d].

In the $Fe(1)O_6$ octahedra the Fe(1) ion is bonded to the $O(1)^{i}$, $O(1)^{ii}$, $O(2)^{i}$, $O(2)^{ii}$ and $O(3)^{i}$, $O(3)^{ii}$ oxygen atoms, belonging to the $HP(1)O_3$ tetrahedra, with similar bond distances of 2.168(3) $(\times 2)$ Å, 2.170(3) $(\times 2)$ Å and 2.171(3) $(\times 2)$ Å, respectively. The *cis*-O–Fe(1)–O angles range from 82.4(1)° to 97.5(1)°. The *trans*-O–Fe(1)–O angles are of 180°, due to the special position occupied by the Fe(1) ions. The distortion of this polyhedron, from an octahedron ($\Delta = 0$) to a trigonal prism ($\Delta = 1$), quantified by the Muetterties and Guggenberger description [20], is $\Delta = 0.11$, which indicates a topology near to octahedral. In the $Fe(2)O_6$ octahedra the Fe(2) ion is bonded to the $O(1)^{i}$, $O(2)^{ii}$ and $O(3)^{i}$ oxygen atoms, belonging to the $HP(1)O_3$ tetrahedron, with bond distances of 2.229(3) Å, 2.242(3) Å and 2.229(2) Å, respectively. The six-fold coordination around the Fe(2) cation is completed with the O(4), $O(5)^{ii}$ and $O(6)^{ii}$ atoms from the $HP(2)O_3$ tetrahedron, with bond lengths of 2.072(3), 2.066(3) and 2.069(3) Å, respectively. The longer metal-oxygen bond distances correspond to the O(1), O(2) and O(3) oxygen atoms, which are shared between the $Fe(1)O_6$ and

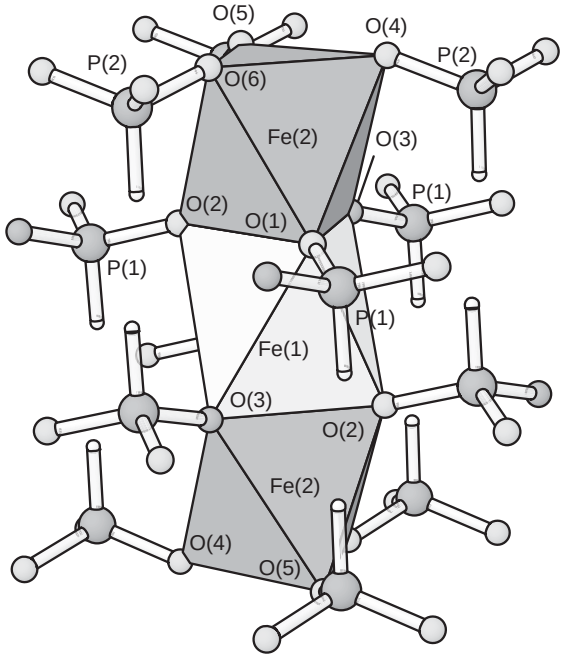

Fig. 3. Polyhedral representation of the Fe_3O_{12} cluster of $(C_2H_{10}N_2)[Fe_3(HPO_3)_4]$ with detailed labeling of the atoms.

$Fe(2)O_6$ octahedra. The *cis*-O–Fe(2)–O angles range from 79.5(1)° to 97.6(1)°. The *trans*-O–Fe(2)–O angles deviate from the ideal value by approximately 8°. The distortion of this polyhedron, from an octahedron ($\Delta = 0$) to a trigonal prism ($\Delta = 1$), is $\Delta = 0.02$, which also indicates a topology near to octahedral. The +2 oxidation state of the iron in the title compound was verified as a sum of bond valences, "*s*", using the formula: $s = \exp[(r_0 - r)/B]$, where $r_0(Fe-O) = 1.734$ Å, $B = 0.37$ Å and "*r*" is the observed bond length [21]. The obtained oxidation states are 1.85 and 1.99 v.u., for Fe(1) and Fe(2), respectively. These values are in good agreement with those expected for this element in the $(C_2H_{10}N_2)[Fe_3(HPO_3)_4]$ chemical formula and confirm the results obtained by X-ray single-crystal structure determination. The $(C_2H_{10}N_2)[Fe_3(HPO_3)_4]$ compound exhibits values of the Fe(II)–O bond distances intermediate between those observed for the isostructural $(C_2H_{10}N_2)[M_3(HPO_3)_4]$ M = Co and Mn phases in accordance with the ionic radii of the Fe, Mn and Co divalent cations [22]. Finally, the Fe–O–Fe angles in the Fe_3O_{12} unit of $(C_2H_{10}N_2)[Fe_3(HPO_3)_4]$ are 82.84(9)°, 82.5(1)° and 82.80(9)° for Fe(1)–O(1)–Fe(2), Fe(1)–O(2)–Fe(2) and Fe(1)–O(3)–Fe(2), respectively, similar to those found in the related manganese(II) and cobalt(II) phases [11b,d]. The Fe(2)–Fe(1)–Fe(2) angle is 180° as observed for all the isostructural phases containing the M_3O_{12} (M = Fe, Mn and Co) trimeric cluster.

The two HPO_3 tetrahedra exhibit similar P–O bond distances, with a mean value of 1.525(4) Å. The H(11)–P(1) and H(22)–P(2) bond distances are equal in both phosphite anions. The O–P–O angles are in the range from 110.7(2)° to 113.9(2)°, while the H–P–O angles range from 102(2)° to 110(2)°. The ethylenediammonium cation exhibits C–C and C–N bond distances in the range usually found for this molecule [11b,11d–g,23] and the angles are similar to those expected for sp^3 hybridization. The ethylenediammonium cation is bonded by hydrogen bonds to the oxygen atoms of the $HP(1)O_3$ anion linking the $[Fe_3(HPO_3)_4]^{2-}$ inorganic sheets, with O–H bond lengths in the 1.91(1)–1.95(1) Å range.

The $(C_2H_{10}N_2)[Fe_3(HPO_3)_4]$ phase has been shown to be isostructural with the recently reported $(C_2H_{10}N_2)[M_3(HPO_3)_4]$ (M = Mn and Co) phases (Table 4) [11b,d]. Refined parameters of the title compound are compared with those of the $(C_2H_{10}N_2)[M_3(HPO_3)_4]$ (M = Mn and Co) compounds in Table 4. Fig. 4 shows the lineal evolution of the cell volume with the M^{2+} radius [22].

Table 4
Unit-cell parameters of the $(C_2H_{10}N_2)[M_3(HPO_3)_4]$ (M = Co, Fe and Mn) compounds, and ionic radii of the metallic cations in hexacoordination

Compound	M = Co	M = Fe	M = Mn
a (Å)	5.351(2)	5.416(1)	5.459(1)
b (Å)	5.347(4)	5.416(1)	5.460(2)
c (Å)	14.016(6)	13.977(2)	14.194(3)
α (°)	80.98(5)	80.64(2)	80.65(2)
β (°)	85.66(4)	85.25(1)	85.45(1)
γ (°)	60.04(4)	60.03(1)	60.04(2)
V(Å)^3	343.0(3)	350.5(1)	361.7(2)
Ionic radius	0.745	0.780	0.830

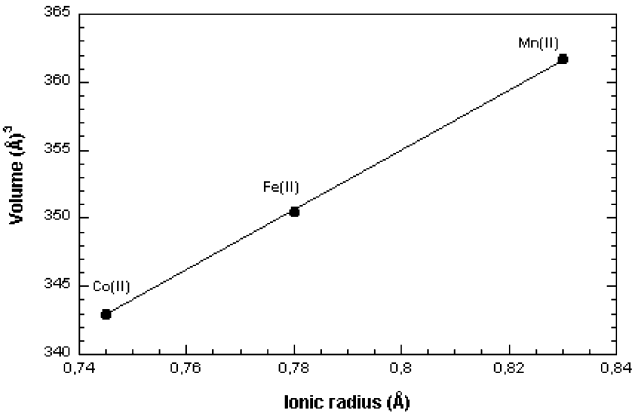

Fig. 4. Variation of the unit-cell volume vs. ionic radius for the $(C_2H_{10}N_2)[M_3(HPO_3)_4]$, M = Co, Fe and Mn, compounds.

3.2. Infrared, UV-visible and Mössbauer spectroscopies

The Infrared spectrum of $(C_2H_{10}N_2)[Fe_3(HPO_3)_4]$ shows the characteristic bands of the protonated ethylenediamine molecule [11b,11d–g,23,24] and the $(HPO_3)^{2-}$ phosphite oxoanion (see Table 5). The results obtained are similar to those found for other related phosphite phases containing the ethylenediammonium cation as templating agent [11b–g].

In the diffuse reflectance spectrum, two bands at approximately 6860 and 9265 cm^{-1} are observed, which are characteristic of the iron(II) d^6 high spin cation in a slightly distorted octahedral environment. The bands correspond to the electronic transitions from the $^5T_{2g}(^5D)$ fundamental state to the excited level $^5E_{2g}(^5D)$ [25,26] which is splitted as consequence of the Jahn–Teller effect expected for this cation. The energy associated with this transition corresponds, according to the Tanabe–Sugano diagram, to the Dq parameter. The value obtained is $Dq = 805\ cm^{-1}$, in good agreement with the values observed in other related compounds containing the Fe^{2+} metallic cation [27].

The Mössbauer spectrum recorded in the paramagnetic state at 300 K is typical of high-spin ferrous ions (Fig. 5). The spectrum exhibits two symmetric doublets.

Table 5
Selected IR bands (values in cm^{-1}) of $(C_2H_{10}N_2)[Fe_3(HPO_3)_4]$

Assignment	
$\nu(-NH_3)^+$	2890 (m)
$\nu(-CH_2-)$	2800 (m)
ν(HP)	2510, 2475 (m)
$\delta(-NH_3)^+$	1590, 1620 (m,s)
$\delta(-CH_2-)$	1470 (w)
$\nu_{as}(PO_3)$	1140, 1085 (s)
δ(HP)	1070, 1045 (s)
$\nu_s(PO_3)$	990 (m)
$\delta_s(PO_3)$	645, 620 (m)
$\delta_{as}(PO_3)$	490 (m)

ν = stretching, δ = deformation, s = symmetric, as = asymmetric; s = strong, m = medium, w = weak.

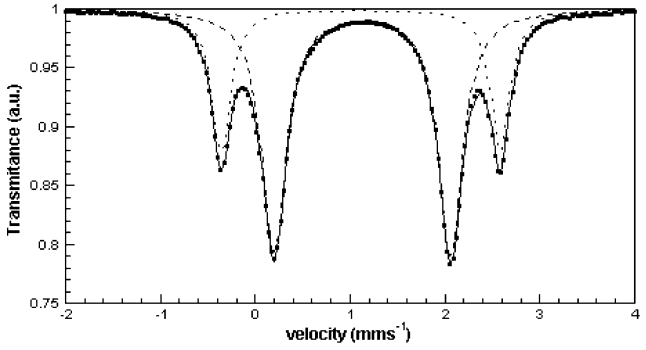

Fig. 5. Mössbauer spectrum of $(C_2H_{10}N_2)[Fe_3(HPO_3)_4]$ at 300 K.

Table 6
Isomer shift (IS) relative to α-Fe metal, quadrupole splitting (QS) and relative spectral areas (RSA) of the ^{57}Fe Mössbauer spectrum of $(C_2H_{10}N_2)[Fe_3(HPO_3)_4]$ at 300 K.

Site	IS (mm s^{-1})	QS (mm s^{-1})	RSA (%)
Fe(1)	1.2230(5)	2.942(1)	31.4(1)
Fe(2)	1.2391(1)	1.8606(2)	68.6(1)

Taking into account the existence of the two crystallographically independent iron(II) cations in $(C_2H_{10}N_2)[Fe_3(HPO_3)_4]$, the spectrum was fitted by two doublets of Lorentzians using the NORMOS program [28]. The values obtained for the isomer shift and the quadrupole splitting are characteristic of Fe(II) (Table 6). The relative spectral areas are approximately in the 1:2 ratio of the Fe(1) and Fe(2) cations, respectively. This result confirms the existence of nonequivalent positions for the iron(II) cations obtained from single crystal X-ray structural refinement.

3.3. Magnetic properties

Magnetic susceptibility of $(C_2H_{10}N_2)[Fe_3(HPO_3)_4]$ was measured on a powdered sample from room temperature to 5.0 K. The plot of the thermal evolution of χ_m and $\chi_m T$ is displayed in Fig. 6.

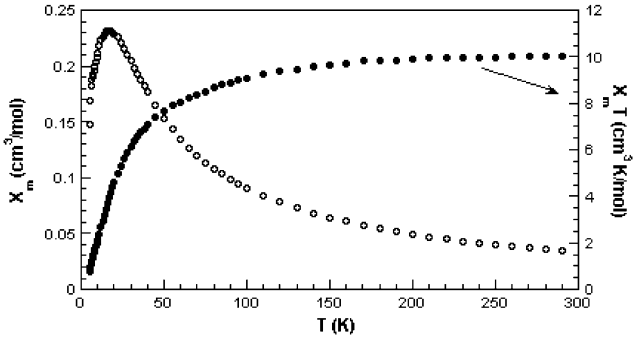

Fig. 6. Thermal evolution of χ_m and $\chi_m T$ curves of $(C_2H_{10}N_2)[Fe_3(HPO_3)_4]$.

The molar magnetic susceptibility, χ_m, increases with decreasing temperature, reaches a maximum at approximately 16.0 K, indicating that an antiferromagnetic ordering is established at this temperature. After 16 K the susceptibility decreases to 0.148 emu/mol at 5.0 K. At high temperatures ($T > 50$ K) the χ_m vs. T curve follows a Curie–Weiss law, with values of the Curie and Curie–Weiss constants of $C_m = 10.734\,cm^3K/mol$ and $\theta = -18.3$ K, respectively. The effective magnetic moment and the g-value calculated from the Curie constant are 5.3 μ_B and 2.2, respectively. These values are in the range habitually found for other iron(II) compounds [29]. The value of the effective magnetic moment is slightly higher than that of the spin only moment (4.9 μ_B) due to the orbital contribution from the metallic cation [29]. The $\chi_m T$ vs. T product decreases from 10.085 emuK/mol at room temperature up to, approximately, 0.894 emuK/mol at 5.0 K. Both the continuous decrease of the $\chi_m T$ vs. T curve and the negative Weiss temperature indicate the existence of antiferromagnetic interactions in this compound.

4. Concluding remarks

A new organically templated phase of formula $(C_2H_{10}N_2)[Fe_3(HPO_3)_4]$ has been prepared in the form of single crystals using mild hydrothermal conditions. The phase exhibits a layered structure in which the sheets are formed by Fe_3O_{12} trimeric units sharing faces. The IR spectroscopy has corroborated the existence of the phosphite oxoanions and the ethylenediammonium cations. The Dq parameter obtained by electronic spectroscopy in the visible region is consistent with iron(II) cations in octahedral coordination. The Mössbauer spectrum shows the presence of two doublets characteristic of the presence in the compound of two

crystallographically independent iron(II) cations. The magnetic measurements are consistent with the existence of an antiferromagnetic behavior.

Acknowledgments

This work was financially supported by the Ministerio de Educación y Ciencia (BQU2001-0678) and Universidad del País Vasco/EHU (9/UPV00169.310-13494/2001; 9/UPV00130.310-13700/2001), which we gratefully acknowledge. U-Chan Chung and Jon P. Chapman thanks the Universidad del País Vasco and the Ministerio de Educación y Ciencia (MAT2001), respectively, for funding.

References

[1] (a) N.K. Raman, M.T. Anderson, C.J. Brinker, Chem. Mater. 8 (1996) 1682;
(b) S. Mann, S.L. Burkett, S.A. Davis, C.E. Fowler, N.H. Mendelson, S.D. Sims, S.D. Walsh, N.T. Whilton, Chem. Mater. 9 (1997) 2300;
(c) L.A. Estroff, A.D. Hamilton, Chem. Mater. 13 (2001) 3227;
(d) S.A. Davis, N. Breulmann, K.H. Rhodes, B. Zhang, S. Mann, Chem. Mater. 13 (2001) 3218;
(e) R.A. Caruso, M. Antonietti, Chem. Mater. 13 (2001) 3272.
[2] A.K. Cheetham, G. Ferey, T. Loiseau, Angew. Chem., Int. Ed. 38 (1999) 3268.
[3] M.E. Davis, R.F. Lobo, Chem. Mater. 4 (1992) 756.
[4] S.L. Lawton, W.J. Rohrbaugh, Science 247 (1990) 1319.
[5] (a) E.M. Flanigen, Stud. Surf. Sci. Catal. 137 (2001) 11;
(b) J.D. Sherman, Proc. Natl. Acad. Sci. USA 96 (1999) 3471.
[6] (a) R.M. Barrer, Hydrothermal Chemistry of Zeolites, Academic Press, New York, 1989;
(b) W.M. Meier, D.H. Olson, Atlas of Zeolite Structure Types, Elsevier, London, 1996.
[7] S.T. Wilson, B.M. Lok, C.A. Messina, T.R. Cannon, E.M. Flanigen, J. Am. Chem. Soc. 104 (4) (1982) 1146.
[8] (a) J.B. Parise, Inorg. Chem. 24 (1985) 4312;
(b) G. Ferey, J. Fluorine Chem. 72 (1995) 187;
(c) D.M. Chapman, A.L. Rol, Zeolites 10 (1990) 730;
(d) T.E. Gier, G.D. Stucky, Nature 349 (1991) 508;
(e) G.Y. Yang, S.C. Sevov, J. Am. Chem. Soc. 121 (1999) 8389;
(f) P. Feng, X. Bu, G.D. Stucky, Nature 388 (1997) 735;
(g) M. Cavellec, D. Riou, C. Ninclaus, J.M. Greneche, G. Ferey, Zeolites 17 (1996) 260;
(h) K.-H. Lii, Y.-F. Huang, V. Zima, C.-Y. Huang, H.-M. Lin, Y.-C. Jiang, F.-L. Liao, S.-L. Wang, Chem. Mater. 10 (1998) 2599;
(i) V. Soghomoniam, Q. Chen, R.C. Haushalter, J. Zubieta, Angew. Chem. Int. Ed. Engl. 34 (1995) 223;
(j) N. Guillou, Q. Gao, M. Nogues, R.E. Morris, M. Hervieu, G. Ferey, A.K. Cheetham, C. R. Acad. Sci. Paris Ser. 2 (1999) 387;
(k) R. Haushalter, L.A. Mundi, Chem. Mater. 4 (1992) 31.
[9] (a) M. Cavellec, D. Riou, J.M. Greneche, G. Ferey, Inorg. Chem. 36 (1997) 2181;
(b) J.R.D. DeBord, W.M. Reiff, C.J. Warren, R. Haushalter, J. Zubieta, Chem. Mater. 9 (1997) 1994;
(c) K.H. Lii, Y.F. Huang, J. Chem. Soc., Chem. Commun. (1997) 1311;
(d) V. Zima, K.-H. Lii, N. Nguyen, A. Ducouret, Chem. Mater. 10 (1998) 1914;
(e) J. DeBord, W. Reiff, R. Haushalter, J. Zubieta, J. Solid State Chem. 125 (1996) 186;
(f) K.-H. Lii, Y.-F. Huang, J. Chem. Soc., Dalton Trans. (1997) 2221.
[10] (a) F. Sapiña, P. Gomez, M.D. Marcos, P. Amoros, R. Ibañez, D. Beltran, Eur. J. Solid State Inorg. Chem. 26 (1989) 603;
(b) M.D. Marcos, P. Amoros, A. Beltran, R. Martinez, J.P. Attfield, Chem. Mater. 5 (1993) 121;
(c) M.P. Attfield, R.E. Morris, A.K. Cheetham, Acta Crystallogr. C 50 (1994) 981;
(d) M.D. Marcos, P. Amoros, A. Le Bail, J. Solid State Chem. 107 (1993) 250.
[11] (a) G. Bonavia, J. DeBord, R.C. Haushalter, D. Rose, J. Zubieta, Chem. Mater. 7 (1995) 1995;
(b) S. Fernandez, J.L. Mesa, J.L. Pizarro, L. Lezama, M.I. Arriortua, R. Olazcuaga, T. Rojo, Chem. Mater. 12 (2000) 2092;
(c) S. Fernandez, J.L. Pizarro, J.L. Mesa, L. Lezama, M.I. Arriortua, R. Olazcuaga, T. Rojo, Inorg. Chem. 40 (2001) 3476;
(d) S. Fernandez, J.L. Pizarro, J.L. Mesa, L. Lezama, M.I. Arriortua, T. Rojo, Int. J. Inorg. Mater. 3 (2001) 331;
(e) S. Fernandez, J.L. Mesa, J.L. Pizarro, L. Lezama, M.I. Arriortua, T. Rojo, Chem. Mater. 14 (2002) 2300;
(f) S. Fernandez, J.L. Mesa, J.L. Pizarro, L. Lezama, M.I. Arriortua, T. Rojo, Angew. Chem., Int. Ed. 41 (2002) 3683;
(g) S. Fernandez, J.L. Mesa, J.L. Pizarro, L. Lezama, M.I. Arriortua, T. Rojo, Chem. Mater. 15 (2003) 1204;
(h) S. Fernandez, J.L. Mesa, J.L. Pizarro, J.S. Garitaonandia, M.I. Arriortua, T. Rojo, Angew. Chem. Int. Ed. 43 (2004) 977.
[12] (a) J. Rodriguez-Carvajal, FULLPROF Program for Rietveld Refinement and Pattern Matching Analysis of Powder Patterns, 1998, unpublished;
(b) D.B. Wiles, R.A. Young, J. Appl. Crystallogr. 14 (1981) 19.
[13] (a) Powder Diffraction File—Inorganic and Organic, ICDD, File No. 84-0876, Pennsylvania, USA, 1995;
(b) Powder Diffraction File—Inorganic and Organic, ICDD, File No. 30-0659, Pennsylvania, USA, 1995;
(c) Powder Diffraction File—Inorganic and Organic, ICDD, File No. 36-0318, Pennsylvania, USA, 1995.
[14] A.C.T. North, D.C. Philips, F.S. Mathews, Acta Crystallogr. A 24 (1968) 351.
[15] A. Chandrasekaran, X-RAYACS: Program for Single Crystal X-ray Data Corrections; Chemistry Department, University of Massachusetts, Amherst, USA, 1998.
[16] G.M. Sheldrick, SHELXS 97: Program for the Solution of Crystal Structures; University of Göttingen, Germany, 1997.
[17] G.M. Sheldrick, SHELXL 97: Program for the Refinement of Crystal Structures, University of Göttingen, Germany, 1997.
[18] International Tables for X-ray Crystallography. Vol. IV, Kynoch Press, Birmingham, England, 1974, p. 99.
[19] E. Dowty, ATOMS: A Computer Program for Displaying Atomic Structures; Shape Software, 521 Hidden Valley Road, Kingsport, TN, 1993.
[20] E.L. Muetterties, L.J. Guggenberger, J. Am. Chem. Soc. 96 (1974) 1748.
[21] I.D. Brown, in: M. O'Keeffe, A. Navrotsky (Eds.), Structure and Bonding in Crystals, Vol. 2, Academic Press, New York, 1981, p. 1.
[22] R.D. Shannon, Acta Crystallogr. A 32 (1976) 751.

[23] A. Gharbi, A. Jouini, M.T. Averbuch-Pouchot, A. Durif, J. Solid State Chem. 111 (1994) 330.
[24] D. Dolphin, A.E. Wick, Tabulation of Infrared Spectral Data, Wiley, New York, 1977.
[25] Y. Tanabe, S.J. Sugano, Phys. Soc. Japan 9 (1954) 753.
[26] J.E. Orgel, J. Chem. Phys. 23 (1955) 1004.
[27] A.B.P. Lever, Inorganic Electronic Spectroscopy, Elsevier Science Publishers B.V., Amsterdam, Netherlands, 1984.
[28] R.A. Brand, J. Larner, D.M. Herlach, J. Phys. F 14 (1984) 555.
[29] R.L. Carlin, Magnetochemistry, Springer, Berlin, 1986.